Ultrafast laser-induced changes of the magnetic anisotropy in a low-symmetry iron garnet film

L. A. Shelukhin, V. V. Pavlov, P. A. Usachev, P. Yu. Shamray, R. V. Pisarev, and A. M. Kalashnikova*
Ioffe Institute, 194021 St. Petersburg, Russia

(Received 8 November 2017; published 19 January 2018)

We explore a thermal mechanism of changing the magnetic anisotropy by using femtosecond laser pulses in a low-symmetry dielectric ferrimagnetic garnet $(YBiPrLu)_3(FeGa)_5O_{12}$ film grown on the (210)-type $Gd_3Ga_5O_{12}$ substrate as a model media. Employing spectral magneto-optical pump-probe technique and phenomenological analysis, we demonstrate that the magnetization precession in this film is a result of laser-induced changes of the growth-induced magnetic anisotropy along with the ultrafast inverse Faraday effect. The change of magnetic anisotropy relies on the lattice heating induced by laser pulses of any polarization on a picosecond time scale. We show that the orientation of the external magnetic field with respect to the magnetization easy plane affects the precession noticeably. Importantly, the relative contributions from the ultrafast inverse Faraday effect and the change of different growth-induced anisotropy parameters can be controlled varying the applied magnetic field strength and direction. As a result, the amplitude and the initial phase of the excited magnetization precession can be gradually tuned.

DOI: 10.1103/PhysRevB.97.014422

I. INTRODUCTION

Ferrimagnetic rare-earth iron garnets $R_3Fe_5O_{12}$ and related compounds, where R stands for yttrium, rare-earth, and some other ions, e.g., bismuth, are highly resistive dielectrics with the band gap of $E_g \sim 2.8$ eV. These materials have passed through several periods of strong research interest, triggered by their unique physical properties and important applications [1,2]. First of all, yttrium iron garnet (YIG) possesses a record-narrow width of the ferromagnetic resonance line [3] and the strong magnetoacoustic coupling [4], thus being a basic medium for a large family of microwave devices. Being centrosymmetric cubic in the bulk, epitaxial magnetic garnet films reduce their crystallographic symmetry and generally lose the center of inversion, which allows for various effects forbidden in cubic bulk samples, such as the optical second-harmonic generation [5,6] and intrinsic giant linear magnetoelectric effect [7–9]. Owing to the piezomagnetic response, thin magnetic garnet films are among the building blocks for composite multiferroics as well [10]. High values of Faraday rotation in Bi-substituted YIG allow designing efficient magneto-optical isolators and waveguides [11]. The same property makes magnetic garnets the key material for engineering magnetophotonic [12] and magnetoplasmonic [13,14] structures. Thin magnetic garnet films with uniaxial anisotropy were among the model media for developing magnetic bubble domain technology [15,16], and became of interest recently again owing to certain analogies between bubble domains and skyrmions [17], and to the possibility of controlling domain walls by localized electric fields [18,19]. Nowadays, thin YIG films are the model functional media for testing various concepts of magnonics [20], owing to their exceptionally low spin waves damping [21], and novel effects at the dielectric garnet/metal interfaces [22].

This outstanding functionality of the magnetic garnet films originates from the fact that their magnetization, magnetic anisotropy, compensation points, and other properties can be tailored in a wide range. Thus, growth conditions, a type of substrate, and a chemical composition allows fabricating the garnets with easy-plane, out-of-plane, and more intricate types of the anisotropy [1,2]. Furthermore, the magnetic anisotropy of garnets is highly susceptible to various external stimuli, such as temperature [23], strain [10], and optical irradiation [24,25]. As a result, efficient dynamical modulation of parameters of ferromagnetic resonance and spin waves spectra, domain patterns, etc. can be realized by using these external stimuli. Recently, the control of the magnetic anisotropy of garnet films was demonstrated by means of femtosecond laser pulses, thus showing the feasibility of ultrafast photomagnetic effects [26].

By now, femtosecond laser-induced changes of the magnetic anisotropy has been shown to be one of the most common effects, observed in magnetically ordered dielectrics [26–29], semiconductors [30,31], and metals [32–34]. In all substances, ultrafast change of the intrinsic magnetocrystalline and shape anisotropies by femtosecond laser pulses or the appearance of a transient laser-induced anisotropy axis manifest themselves via coherent spin precession, despite very different microscopic mechanisms underlying these processes, and related, first of all, to the corresponding electronic band structures. For example, excitation by a femtosecond laser pulse of magnetically ordered metals results in a subpicosecond increase of the electronic temperature which determines the subsequent dynamics of other subsystems [35–37]. Therefore, in such media changes of the shape and magnetocrystalline anisotropies mostly result from the ultrafast heating [32,33] and related effects [34]. By contrast, magnetically ordered dielectrics subjected to femtosecond laser pulses demonstrate a variety of both thermal and nonthermal mechanisms leading to the anisotropy changes.

The most prominent nonthermal changes of the magnetic anisotropy in dielectrics under the action of laser pulses were

*kalashnikova@mail.ioffe.ru

observed in several substituted iron garnets [26,29,38,39], in which linearly polarized pulses induce a transient anisotropy axis due to charge-transfer optical transitions. These results demonstrated the feasibility of controlling the magnetic anisotropy by changing the azimuthal angle of the laser pulse polarization. Furthermore, this ultrafast photomagnetic effect allowed achieving relatively high amplitudes of laser-induced magnetization precession [38] and even controllable switching of magnetization [29]. Recently, impulsive photomagnetic effect has been discussed in Ref. [40] as another candidate for triggering the magnetization precession in a magnetic garnet, for which a microscopical picture is yet to be understood. The laser-induced uniaxial anisotropy mediated by the acoustic phonons has been shown to enhance magnetization of the Cu-based organic-inorganic Heisenberg magnets [28].

Rapid heating related to the laser pulses can also lead to a modification of the intrinsic magnetocrystalline anisotropy of dielectrics. Exploring this mechanism in the rare-earth orthoferrites in the vicinity of spin reorientation phase transitions [27] yielded a number of remarkable results on coherent control of magnetization [41–43]. Evidently, laser-induced thermal change of the magnetic anisotropy should be a general phenomenon in dielectrics, not restricted exclusively to the vicinity of phase transitions. Such a process, therefore, can be an alternative way to the spin waves excitation. Thermal modulation of the anisotropy can affect the spin waves spectrum and other dynamical properties and, therefore, understanding the time scales and strength of this effect in dielectrics is important for the implementation of laser pulses as excitation stimuli in future magnonic [44], magnetoplasmonic [45,46], spintronic, and spin-optronic devices. However, to the best of our knowledge, ultrafast thermal changes of magnetic anisotropy of dielectrics, except for orthoferrites [27,41–43,47,48], have not been explored so far.

In this paper we report on the results of the experimental studies of ultrafast magnetization dynamics in a low-symmetry substituted iron garnet film characterized by a pronounced growth-induced anisotropy of the easy-axis type. We demonstrate that the impact of a femtosecond laser pulse on the garnet film induces polarization-independent changes of its growth-induced anisotropy parameters. Their relative contributions can be distinguished by analyzing the azimuthal field dependencies of the initial phase of the induced precession owing to the low symmetry. We argue that the most plausible mechanism underlying the observed change of the magnetic anisotropy is the lattice heating, which is expected to take place on a picosecond time scale. We show that the amplitude of the magnetization precession excited via this mechanism is comparable to that induced by the ultrafast inverse Faraday effect. The relative contribution of these two mechanisms of the magnetization precession excitation can be tuned by changing the value of the applied magnetic field. Importantly, this allowed us to vary gradually the initial phase of the magnetization precession in the range of $\sim\pi/2$.

The paper is organized as follows. In Sec. II we introduce a phenomenological description of the magnetic anisotropy of the substituted iron garnet film grown on (210)-type substrate. We consider how the ultrafast change of the magnetic anisotropy parameters is expected to affect the magnetic state of the low-symmetry garnet film. Section III is dedicated to the characterization of the magnetic garnet film chosen for the study. In Sec. IV we present the details of the magneto-optical pump-probe experiments. In Sec. V A the experimental data on the magnetization dynamics after the laser pulse excitation in the (210)-type film are discussed. This is followed by the analysis of two mechanisms of the precession excitation: the ultrafast inverse Faraday effect (Sec. V B) and change of the growth-induced anisotropy parameters under the influence of laser pulses (Sec. V C).

II. MAGNETIC ANISOTROPY OF A GARNET FILM GROWN ON A (210)-TYPE SUBSTRATE

Substituted iron garnet films are characterized by the magnetic anisotropy originating from the interplay between cubic anisotropy inherent to their crystallographic structure and the growth- and stress-induced ones. These latter two depend on several factors such as substrate lattice parameters and crystallographic orientation, particular chemical composition of a film, and parameters of the growth technology (for a review, see, e.g. Refs. [15,49]). Typically, in films grown on low-symmetry substrates the growth- and/or stress-induced contributions dominate, which results in magnetic anisotropy of the easy-axis type.

We consider here a magnetic garnet film grown on the (210)-type substrate. The reference frame is chosen as shown in Fig. 1(a). The x axis is directed along the [001] crystallographic direction. From the symmetry point of view this direction is the $\bar{2}_x$ axis and the crystallographic point group of this film is m [6]. The z axis is directed along the [210] crystallographic axis and is normal to the sample plane. The magnetic anisotropy energy of such a film can be expressed as [15,50] (see also Appendix A)

$$w_{\mathrm{a}} = K_u m_z^2 + K_i m_y^2 + K_{yz} m_y m_z + w_{\mathrm{cub}}, \qquad (1)$$

where $m_k = M_k/M_S$ $(k = x,y,z)$ are the normalized components of the magnetization $\mathbf{M}$, and M_S is the saturation magnetization. In this expression w_{cub} is the cubic anisotropy energy; K_u, K_i, and K_{yz} are the uniaxial out-of-plane, in-plane, and orthorhombic anisotropy parameters, respectively. The first three terms in Eq. (1) have two contributions: the growth-induced and the stress-induced ones. The relative strength of these contributions varies depending on the composition of a particular film, film/substrate lattice mismatch, and the growth conditions. In particular, in Bi-substituted iron garnets, investigated in our experiments, the growth-induced anisotropy due to Bi^{3+} ions occupying dodecahedral sites dominates over the stress-induced one [51], as we discuss in more detail in Appendix A. The cubic anisotropy w_{cub} is typically much weaker than the growth-induced one, and is omitted in the following consideration.

The equilibrium orientation of the magnetization is determined by the ratios between magnetic anisotropy parameters entering Eq. (1). In particular, the yz plane is the easy plane of the magnetization, given $K_{yz} < 0$. The orientation of the magnetization in this plane is determined by the values of K_u, K_i, and K_{yz}. The expression for the effective magnetic

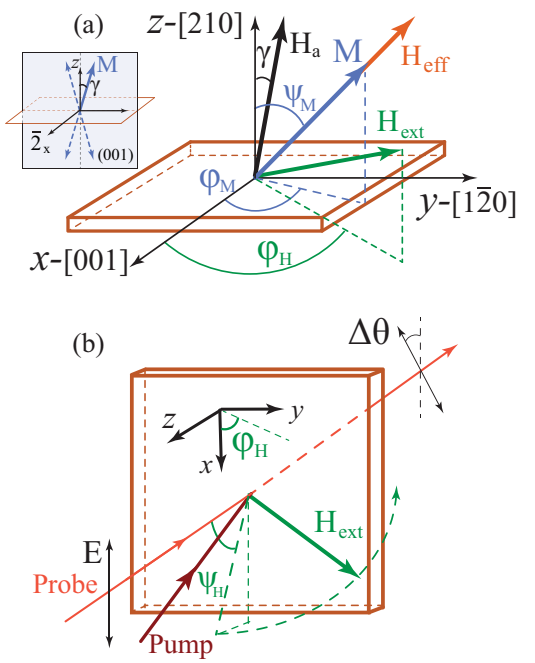

FIG. 1. (a) Orientations of the crystallographic axes in the (210)-film, the applied magnetic field $\mathbf{H}_{\text{ext}}$, the effective anisotropy field $\mathbf{H}_{\text{a}}$, and the net effective field $\mathbf{H}_{\text{eff}}$. x,y,z axes are directed along the [001], [1$\bar{2}$0], and [210] crystallographic axes, respectively. Effective anisotropy field $\mathbf{H}_{\text{a}}$ makes an angle $\gamma = 16^{\text{o}}$ with the z axis in the yz plane [7], as shown in the inset. The magnetic field direction is described by the polar angle $\psi_{\text{H}} = 80^{\text{o}}$ and the azimuthal angle φ_{H}. The direction of magnetization $\mathbf{M}$ is described by the polar ψ_{M} and azimuthal φ_{M} angles. In a general case the magnetization $\mathbf{M}$ is not collinear with the applied magnetic field and is not in the yz plane. (b) Geometry of the pump-probe experiment (see text for the details).

anisotropy field $\mathbf{H}_{\text{a}}$ has a form

$$\mathbf{H}_{\text{a}} = -\frac{\partial w_{\text{a}}}{\partial \mathbf{M}} = \frac{1}{M_S^2}\begin{pmatrix} 0 \\ -2K_i M_y - K_{yz} M_z \\ -2K_u M_z - K_{yz} M_y \end{pmatrix}. \quad (2)$$

From this expression one can see that a laser-induced change of the anisotropy parameters K_u, K_i, or K_{yz} should lead to changes of both the value and the direction of the effective anisotropy field. In order to illustrate how changes of these parameters can lead to the excitation of the magnetization precession, we employ the phenomenological approach based on the Landau-Lifshitz-Gilbert (LLG) equation [52,53]

$$\frac{d\mathbf{M}}{dt} = -\gamma \mathbf{M} \times \mathbf{H}_{\text{eff}} + \frac{\alpha}{\mathbf{M}}\left(\mathbf{M} \times \frac{d\mathbf{M}}{dt}\right)$$
$$= -\gamma \mathbf{M} \times (\mathbf{H}_{\text{ext}} + \mathbf{H}_{\text{a}} + \mathbf{H}_{\text{d}}) + \frac{\alpha}{\mathbf{M}}\left(\mathbf{M} \times \frac{d\mathbf{M}}{dt}\right), \quad (3)$$

where γ is the gyromagnetic ratio, α is the Gilbert damping factor, and $\mathbf{H}_{\text{eff}}$ is the net effective magnetic field, which is a sum of the applied magnetic field $\mathbf{H}_{\text{ext}}$, the internal anisotropy field $\mathbf{H}_{\text{a}}$, and the demagnetizing field $\mathbf{H}_{\text{d}} = -4\pi M_z \mathbf{z}$.

In this approach the effect of the femtosecond laser pulse is introduced into the LLG equation (3) by modifying expression for the effective magnetic field $\mathbf{H}_{\text{eff}}$. In particular, (i) the change of the anisotropy parameters $\Delta K_u(t)$, $\Delta K_i(t)$, and $\Delta K_{yz}(t)$ manifests itself in the change of the effective anisotropy field $\Delta \mathbf{H}_{\text{a}}(t)$ and (ii) the effective field $\mathbf{H}_{\text{om}}(t)$ accounts for the optomagnetic effects, such as the ultrafast inverse Faraday and Cotton-Mouton effects [54–57].

Using Eqs. (2) and (3) one can derive general expressions for the torque $\mathbf{T}_0$ acting on the magnetization at $t = 0$ due to these effects, assuming that the anisotropy is modified at the sufficiently short time scale:

$$\frac{1}{\gamma}\mathbf{T}_0 = \frac{1}{\gamma}\frac{d\mathbf{M}}{dt}\bigg|_{t=0} = -\mathbf{M} \times (\Delta \mathbf{H}_{\text{a}} + \mathbf{H}_{\text{om}})$$
$$= \begin{pmatrix} \left[2(\Delta K_i - \Delta K_u) m_y m_z + \Delta K_{yz}\left(m_z^2 - m_y^2\right)\right] \\ (2\Delta K_u m_x m_z + \Delta K_{yz} m_x m_y) \\ (-2\Delta K_i m_x m_y - \Delta K_{yz} m_x m_z) \end{pmatrix}$$
$$+ \begin{pmatrix} (H_{\text{om}z} M_y - H_{\text{om}y} M_z) \\ (H_{\text{om}x} M_z - H_{\text{om}z} M_x) \\ (H_{\text{om}y} M_x - H_{\text{om}x} M_y) \end{pmatrix}. \quad (4)$$

Importantly, Eq. (4) clearly demonstrates that the strength and the direction of the torque $\mathbf{T}_0$ acting on the magnetization due to the induced changes of any anisotropy parameters ΔK, as well as due to ultrafast optomagnetic effects are determined by the initial orientation of the magnetization. In Eq. (4) the damping term is omitted, since its contribution can be ignored at $t = 0$ for realistic values of α.

Dependence of the torque $\mathbf{T}_0$ (4) on the initial magnetization direction makes an iron garnet film grown on a (210)-type substrate the model medium to explore experimentally laser-induced changes of the magnetic anisotropy parameters ΔK. Indeed, the external magnetic field $\mathbf{H}_{\text{ext}}$ of variable strength applied along the hard axis x gradually changes the equilibrium orientation of the magnetization. Therefore, this should favor experimental detection of the magnetization dynamics excited due to changes of the anisotropy parameters and, moreover, can allow one to determine their relative contributions. It is also important to emphasize that the magnetization dynamics excited due to such changes would be strongly dependent on the time scale of the involved processes. Generally speaking, it should occur on a time scale shorter than the characteristic time of the magnetization precession. If it is not the case, then one can expect a slow deflection movement of the magnetization toward a new equilibrium position instead of the precessional motion.

We note that, when deriving the expression for the torque $\mathbf{T}_0$ (4), we neglected a possible change of the saturation magnetization $\Delta M_S(t)$ due to the laser-induced demagnetization. This is justified because the optically driven demagnetization in dielectrics triggered by optical pulses below band gap occurs on a time scale of several hundreds of picoseconds [58,59], which is longer than the typical precession period of ~100 ps in magnetic garnet films. Therefore, the demagnetization, although resulting in the changes of demagnetizing field $\Delta \mathbf{H}_{\text{d}}$, is not expected to contribute to the torque $\mathbf{T}_0$ (4). The validity of this assumption was verified experimentally, as discussed in Appendix B.

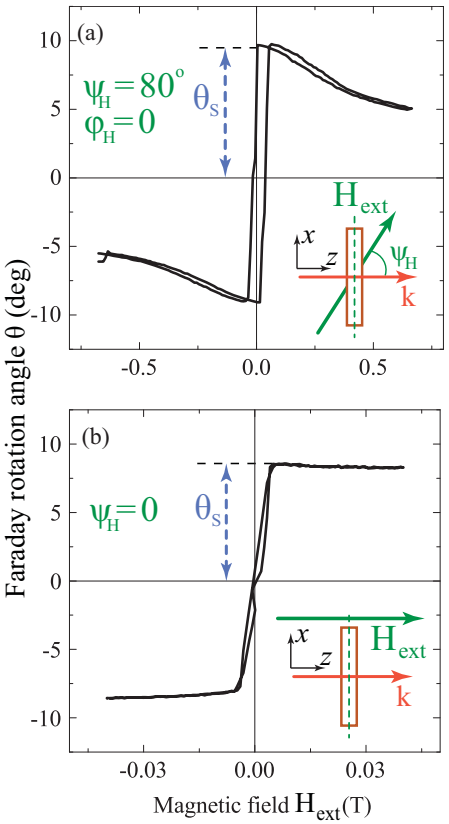

FIG. 2. Static Faraday rotation θ measured as a function of the external magnetic field applied at the angle (a) $\psi_H = 80^o$ and (b) $\psi_H = 0$ with respect to the sample normal (as shown in the insets). θ_s denotes the Faraday rotation at remanence which is proportional to the samples magnetization M_s.

III. SAMPLES

For investigating the feasibility of the described above laser-induced modification of anisotropy parameters we have chosen Bi-substituted iron garnet film $(Y_{0.99}Bi_{1.64}Pr_{0.25}Lu_{0.23})(Fe_{3.75}Ga_{1.16})O_{12}$ grown by the liquid-phase epitaxy method on (210)-type substrate of a gadolinium gallium garnet $Gd_3Ga_5O_{12}$ (GGG). The film composition was verified by the x-ray fluorescence (XRF) measurements. The film thickness was 10 μm. X-ray diffraction characterization yielded the lattice constants of $a^f = 12.5322$ Å and $a^s = 12.4844$ Å for the garnet film and the GGG substrate, respectively. The lattice mismatch between the film and the substrate, introduced according to Ref. [15], is of $\Delta a/a = (a^s - a^f)/a^f = -0.38\%$. Effective anisotropy easy axis is in the yz plane and makes the angle of 16° with the sample normal [7], as shown in Fig. 1(a). Saturation magnetization is of $M_s = 10^4$ A/m [7].

The sample was further characterized by means of static magneto-optical Faraday rotation measurements at a photon energy of 1.8 eV. The rotation angle θ of the polarization plane of the light propagating through the sample normal was measured as a function of the dc magnetic field H_{ext}. In this geometry the measured Faraday rotation θ is proportional to the out-of-plane, or M_z, component of the film magnetization. Figure 2 shows the field dependences of the Faraday rotation measured when the field was applied at the angle 80° with respect to the sample normal (a) and along it (b). The Faraday rotation is $\theta_s = 8^\circ$, which is consistent with high level of Bi substitution leading to an increase of the magneto-optical susceptibility in comparison with unsubstituted YIG [60]. Presented data also confirm that the magnetization easy axis is oriented close to the sample normal. As one can see from Fig. 2(a), the angle between the magnetization and the easy axis gradually increases with the magnitude of the field applied at large angles to the sample normal.

In order to estimate the magnetic anisotropy strength of the studied sample we performed ferromagnetic resonance (FMR) measurements. However, due to the large FMR linewidth no reliable values could be extracted from the measurements. Therefore, we have obtained the magnetic anisotropy parameters of the studied film from the field dependencies of the Faraday rotation [Fig. 2(a)] and of the frequency of the magnetization precession excited in our pump-probe experiments. Magnetic anisotropy parameters were found to be $K_u \sim -5 \times 10^3$ J/m^2, $K_i \sim -3 \times 10^3$ J/m^2, and $K_{yz} \sim -8.7 \times 10^3$ J/m^2. These parameters (see Appendix A and Table II therein for details) have contributions from the growth-induced ($K_u^g \approx -7 \times 10^3$ J/m^3, $K_i^g \approx -3.5 \times 10^3$ J/m^3, $K_{yz}^g \approx -7.7 \times 10^3$ J/m^3) and the stress-induced ones ($K_u^s \approx 2 \times 10^3$ J/m^3, $K_i^s \approx 5 \times 10^2$ J/m^3, $K_{yz}^s \approx -1 \times 10^3$ J/m^3). The growth-induced contribution to the magnetic anisotropy dominates in agreement with previous studies on Bi:YIG with high levels of Bi substitution [51].

IV. EXPERIMENT

All-optical pump-probe experiments were performed employing a technique analogous to that described elsewhere [61]. An optical parametric amplifier (OPA) pumped by the femtosecond regenerative Yb : $KGd(WO_4)_2$ amplifier (RA) produced 170-fs laser pulses with a repetition rate of 5 kHz. Most of the experiments were performed with OPA-generated pump and probe pulses with central photon energies of $E_p = E_{pr} = 1.8$ eV. For the spectrally resolved studies the pulses with $E_{pr} = 1.2$ eV generated directly by the RA were used as the probe pulses. In the latter experiment the central photon energy of the pump pulses E_p generated by the OPA was tuned between 1.7 and 2.0 eV.

All measurements were done in transmission geometry, as shown in Fig. 1(b). Pump pulses were either linearly or circularly polarized. The angle of incidence for the pump pulses was 12°. Pump spot size at the sample was 150 μm and the pump fluence was 7 mJ/cm^2. The pump-induced magnetization dynamics was monitored by measuring the change of the Faraday rotation for the probe pulses as a function of the pump-probe time delay Δt. Linearly polarized probe pulses were incident along the z axis. Probe pulses were focused at the sample to a spot somewhat smaller than the pump. The probe fluence was ~50 times lower than that of the pump.

In this geometry a rotation of the probe polarization plane $\Delta\theta$ is proportional to the change of the magnetization component M_z. Therefore, $\Delta\theta$ normalized by the static Faraday rotation θ_s at remanence (Fig. 2) is the measure of the laser-induced out-of-plane deviation ΔM_z of the magnetization from

its equilibrium orientation. The external magnetic field $\mathbf{H}_{\text{ext}}$ of up to 0.63 T was applied at $\psi_{\text{H}} = 80^\circ$ to the sample normal in order to deflect the magnetization from its easy axis. The azimuthal angle of the applied field φ_{H} could be varied between 0 and 180°. All measurements were performed at $T = 295$ K.

In our experiments the dynamics of the magnetization following the femtosecond laser pulse excitation was studied as a function of the pump polarization and of the sign and magnitude of the applied magnetic field $\pm H_{\text{ext}}$. In order to distinguish helicity-dependent (hd) effects sensitive to the helicity $\sigma^{\pm}$ of the pump pulses and those dependent on the H_{ext} sign (fd) we used the expressions

$$\frac{\Delta\theta_{\text{hd}}}{\theta_s} = \frac{\Delta\theta(\sigma^+; +H_{\text{ext}}) - \Delta\theta(\sigma^-; +H_{\text{ext}})}{2\theta_s}; \quad (5)$$

$$\frac{\Delta\theta_{\text{fd}}}{\theta_s} = \frac{\Delta\theta(p; +H_{\text{ext}}) - \Delta\theta(p; -H_{\text{ext}})}{2\theta_s}, \quad (6)$$

where p stands for a particular pump polarization, and spans from -1 to 0 and to $+1$ for the left-handed, linearly and right-handed polarized pump pulses.

V. RESULTS AND DISCUSSION

A. Laser-induced magnetization precession

Figure 3(a) shows the rotation of the probe polarization induced by the circularly polarized laser pulse as a function of the pump-probe time delay for different values of the magnetic field H_{ext}. Clear oscillations of the probe polarization are observed superimposed on a slowly changing background. The oscillation frequency f increases with the field [Fig. 3(b)]. This indicates that the observed oscillations result from the precession of the magnetization triggered by the pump pulses. Figure 3(c) shows precession frequency f as a function of the azimuthal angle φ_{H} of the external field $H_{\text{ext}} = 0.26$ T [see Fig. 1(a)]. From these results we were able to determine the orientation of the hard magnetization x axis of the sample, as well as estimate the growth-induced anisotropy parameters (see Appendix A). In the following discussion we adopt the frame of reference, where $\varphi_{\text{H}} = 0$ corresponds to the geometry, when the projection of the H_{ext} on the sample plane is parallel to the x axis [Fig. 1(b)].

The central goal of our study is to explore the possibility of excitation of the magnetization precession via laser-induced change of the anisotropy parameters [see Eq. (4)]. Therefore, most of the experiments described below were performed for the field H_{ext} directed close to the sample's hard axis ($\psi_{\text{H}} = 80^\circ$, $\varphi_{\text{H}} = 0$). In this geometry, when the field makes only a small angle of 10° with the hard magnetization x axis, a change of any of the anisotropy parameters ΔK is expected to affect the orientation and the value of the effective field $\mathbf{H}_{\text{eff}} = \mathbf{H}_{\text{a}} + \mathbf{H}_{\text{d}} + \mathbf{H}_{\text{ext}}$, which in turn should result in the finite torque $\mathbf{T}_0$ according to Eq. (4).

For revealing possible mechanisms of the laser-induced precession we have studied the influence of the pump pulses polarization and the sign of H_{ext} on parameters of the excited dynamics of probe polarization. In Fig. 4(a) we plot the time-resolved dynamics of the probe polarization rotation induced by the right- (σ^+) and left-handed (σ^-) pump pulses. Figure 4(b) shows the dynamics induced by the σ^--polarized

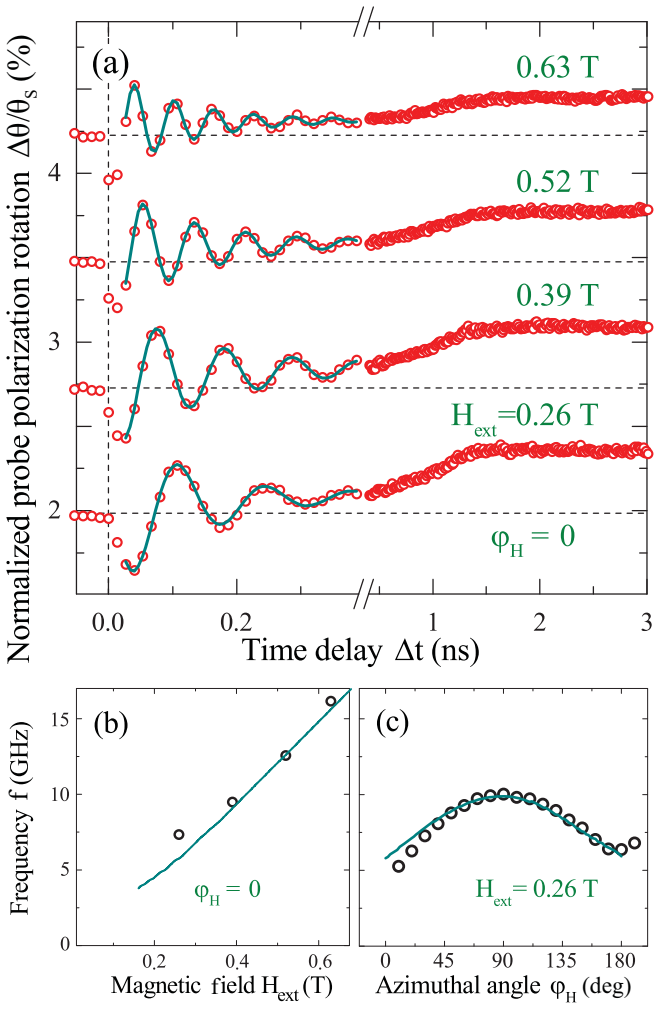

FIG. 3. (a) Normalized rotation of the probe polarization induced by the left-handed (σ^-) circularly polarized pump pulses, measured as a function of the time delay Δt for various magnitudes of the applied magnetic field (symbols). The solid lines represent the best fit in accordance with Eq. (7). (b) Frequency of oscillations in the pump-probe data (a) as a function of the magnetic field magnitude, azimuthal angle $\varphi_{\text{H}} = 0$ (symbols). (c) Frequency of oscillations in the pump-probe data (a) as a function of the magnetic field azimuthal angle φ_{H} (symbols). $H_{\text{ext}} = 0.26$ T. The solid lines in panels (b) and (c) represent the best fit obtained using the analytical expression for magnetic energy [see Appendix A].

pump pulses measured in the positive and negative applied fields of various strengths. One can see that the change of the pump pulse helicity clearly affects the initial phase of the oscillations of M_z in a nontrivial way. In order to evaluate the change of the precession parameters we have fitted the experimental curves shown in Figs. 4(a) and 4(b) by a function

$$\frac{\Delta\theta(t)}{\theta_s} = \frac{\Delta\theta^0}{\theta_s} e^{-t/\tau_{\text{d}}} \cos(2\pi f t + \xi_0) + P_2(t), \quad (7)$$

where $\Delta\theta^0/\theta_s$ is the normalized M_z oscillations amplitude, ξ_0 is the initial phase, τ_{d} is the M_z oscillations decay time, and $P_2(t)$ is the second-order polynomial function accounting for the slowly varying background to be discussed below.

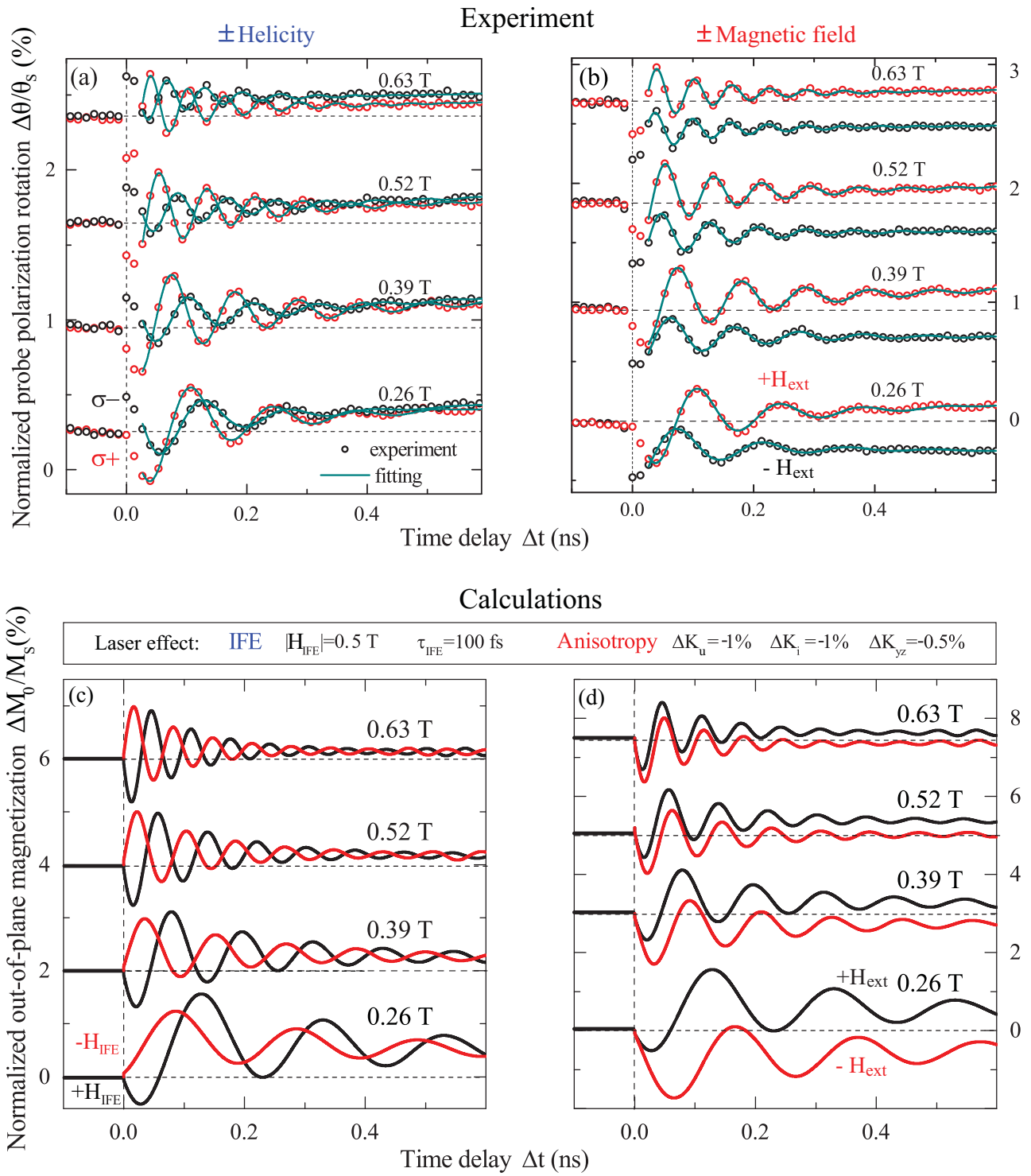

FIG. 4. (a) Normalized probe polarization rotation induced by the left- (σ^-) and right-handed (σ^+) circularly polarized pump pulses as a function of the time delay Δt for the various magnetic fields (symbols). (b) Probe polarization rotation induced by the σ^+-polarized pump pulses as a function of the time delay Δt measured for the various strengths of positive and negative magnetic field $\pm H_{\text{ext}}$ (symbols). The solid lines on panels (a) and (b) represent the best fit in accordance with Eq. (7). (c), (d) Simulation of laser-induced Faraday rotation of probe pulse based on LLG equation (3) for the same cases as (a) and (b), respectively. Parameters used for the simulation are as follows. $\Delta K_u = \Delta K_i = -1\%$; $\Delta K_{yz} = -0.5\%$; $|H_{\text{IFE}}| = 0.5$ T; $\tau_{\text{IFE}} = 100$ fs; $\alpha = 0.1$.

In Fig. 5(a) we plot the initial phase ξ_0 of the precession as a function of H_{ext}. As one can see, the initial phase ξ_0 takes intermediate values in the range of $\sim\pi$, and, furthermore, depends on both the sign and strength of the applied field and the pump polarization. Thus, in the high field limit the change of the pump pulse helicity leads to the change of the initial phase of M_z oscillations by π. As the applied field decreases this helicity-induced change of the initial phase decreases and

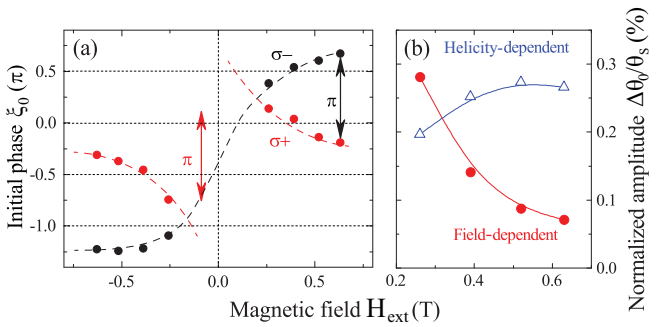

FIG. 5. (a) Initial phase ξ_0 of the probe polarization oscillations excited by $\sigma^{\pm}$-pump pulses as a function of the applied field, as extracted from the experimental data in Fig. 4. (b) Amplitude of the polarization- and field-dependent contributions to the probe polarization oscillations shown in Figs. 4(a) and 4(b) as a function of the applied magnetic field strength.

almost vanishes in the field of $H_{\text{ext}} = 0.26$ T. In contrast, when the pump helicity is fixed but the sign of H_{ext} is reversed, then the phase change by almost π occurs at low fields and vanishes at high fields.

Such a complex behavior suggests that there are two competing mechanisms responsible for the precession excitation. The first one is sensitive to the helicity of the exciting pulse but not to the applied field sign. The second mechanism is independent from the helicity of the laser pulse but is sensitive to the sign of the applied field. In the following discussion we refer to these two mechanisms as helicity-dependent and field-dependent. Their relative contributions depend on the applied magnetic field H_{ext}. This is demonstrated in Fig. 5(b) where we plot the amplitudes of the helicity-dependent $\Delta\theta^0_{\text{hd}}/\theta_s$ and field-dependent $\Delta\theta^0_{\text{fd}}/\theta_s$ contributions to the probe polarization oscillations [Eqs. (5) and (6)].

B. Ultrafast inverse Faraday effect

As discussed above, the helicity-dependent contribution to the laser-induced magnetization precession becomes larger as the applied field increases. This indicates that the contribution is stronger when the the equilibrium magnetization orientation becomes closer to the sample plane, and the angle between $\mathbf{M}$ and the pump wave vector becomes closer to 90°. At the high-field limit ($H_{\text{ext}} = 0.63$ T) the initial phase of the oscillations of the probe polarization is changed by a π when the helicity of the pump pulse is reversed. This allows us to draw the conclusion, that the observed excitation of the magnetization precession occurs via the ultrafast inverse Faraday effect (IFE) [54]. This effect was already detected in garnet films [62–65]. It microscopically originates from the impulsive stimulated Raman scattering on magnons [56,57] and can be described phenomenologically as a femtosecond pulse of an effective magnetic field induced by the circularly polarized laser pulse [54,66,67]

$$\mathbf{H}_{\text{IFE}} \sim \alpha \mathbf{E}(\omega) \times \mathbf{E}(\omega)^* \sim p\varepsilon I_0 \mathbf{z}, \tag{8}$$

where $\mathbf{E}(\omega)$ is the electric field of the light, ε is the magneto-optical susceptibility which also defines the Faraday rotation, and I_0 is the pump intensity. $\mathbf{H}_{\text{IFE}}$ is directed along the wave vector of the pump pulse, i.e., close to the z axis in our experimental geometry [Fig. 1(b)].

In Table I we show the components of the torque $\mathbf{T}_0$ related to $\mathbf{H}_{\text{IFE}}$ as functions of the polar ψ_{M} and azimuthal φ_{M} angles of the magnetization. These components were derived using Eqs. (4) and (8). As one can see, the torque $\mathbf{T}_0$ increases as the angle ψ_{M} between the equilibrium orientation of magnetization and the z axis is increased. In other words, the larger the $M_{x,y}$ components the stronger the created torque (4). This agrees well with the experimental data. Furthermore, the reversal of the applied magnetic field does not affect the initial phase of M_z oscillations excited via IFE [54,56]. This is also in accordance with our experimental data in the high field limit [see Figs. 4(a) and 5(a)]. We note that in Ref. [40] an analogous increase of the precession amplitude excited via IFE with applied field was explained in terms of decreasing demagnetizing field and related ellipticity of the precession trajectory. In our experimental geometry the observed increase of the precession amplitude is dominated by the geometrical effect.

C. Laser-induced changes of the magnetic anisotropy

As opposed to the inverse Faraday effect discussed in the previous section, the efficiency of the helicity-independent mechanism decreases as the applied field is increased. Previous studies have shown that the linearly polarized femtosecond laser pulse can act as the effective field pulse owing to an ultrafast inverse Cotton-Mouton effect, whose microscopical nature is similar to that of IFE [55,56]. Furthermore, linearly polarized pulses can induce transient anisotropy axis in iron garnets and thus excite the magnetization precession [26,29,38–40,62,68]. In order to elucidate a possible microscopic mechanism of the laser-induced precession sensitive to the sign of the applied field, we have verified whether the precession can be excited by the linearly polarized laser pulses, and we have checked whether the azimuthal angle ϕ of the pump polarization affects the excitation process. As shown in Fig. 6(c), the precession can be effectively excited by the linearly polarized pulses.

TABLE I. Components of the torque $\mathbf{T}_0$ arising due to the ultrafast inverse Faraday effect ($\mathbf{H}_{\text{IFE}}$) and the laser-induced changes of the anisotropy parameters ΔK, as functions of the polar and azimuthal angles ψ_{M} and φ_{M}, describing the equilibrium orientation of the magnetization.

Driving mechanism	T_x	T_y	T_z
$\mathbf{H}_{\text{IFE}}$	$T_0^{\text{IFE}} \sin\psi_{\text{M}} \sin\varphi_{\text{M}}$	$-T_0^{\text{IFE}} \sin\psi_{\text{M}} \cos\varphi_{\text{M}}$	0
ΔK_u	$-T_0^{K_u} \sin 2\psi_{\text{M}} \sin\varphi_{\text{M}}$	$T_0^{K_u} \sin 2\psi_{\text{M}} \cos\varphi_{\text{M}}$	0
ΔK_i	$T_0^{K_i} \sin 2\psi_{\text{M}} \sin\varphi_{\text{M}}$	0	$-T_0^{K_i} \sin^2\psi_{\text{M}} \sin 2\varphi_{\text{M}}$
ΔK_{yz}	$T_0^{K_{yz}} \cos^2\psi_{\text{M}} - \sin^2\psi_{\text{M}} \sin^2\varphi_{\text{M}}$	$\frac{1}{2} T_0^{K_{yz}} \sin^2\psi_{\text{M}} \sin 2\varphi_{\text{M}}$	$-\frac{1}{2} T_0^{K_{yz}} \sin 2\psi \cos\varphi_{\text{M}}$

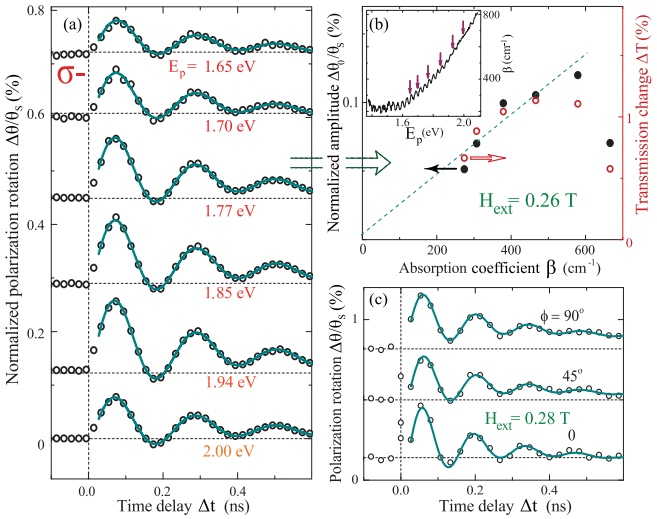

FIG. 6. (a) Normalized probe polarization rotation induced by the left-handed circularly σ^--polarized pump pulses of different photon energy measured as a function of the time delay Δt at $H_{\text{ext}} = 0.26$ T applied along the hard axis (symbols). (b) Normalized magnetization precession amplitude (solid symbols) and transmission change (open symbols) of the probe beam as a function of absorption coefficient β at the pump photon energy E_p. The inset depicts the absorption coefficient as a function of photon energy of the pump. Apparent oscillations in the inset result from the interference of the light in the garnet film. Arrows show the pump photon energies E_p used to obtain the results in panel (a). (c) Normalized probe polarization rotation induced by the linearly polarized pump pulses for different azimuthal angles of pump polarization plane ϕ with respect to the (001) crystallographic direction of the film measured as a function of the time delay Δt at $H_{\text{ext}} = 0.28$ T directed along the hard axis (symbols). The solid lines on panels (a) and (c) represent the best fit in accordance with Eq. (7).

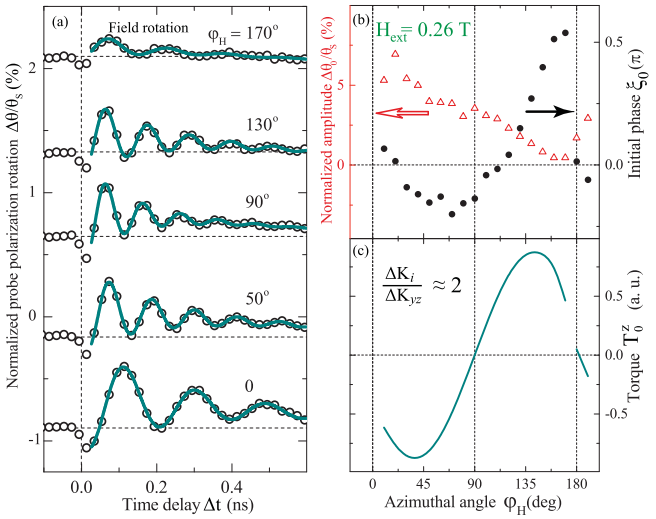

FIG. 7. (a) Normalized probe polarization rotation induced by the left-circularly σ^--polarized pump pulses of different azimuthal angles φ measured as a function of the time delay Δt (symbols). The solid lines represent the best fit in accordance with Eq. (7). (b) Initial phase ξ_0 (solid symbols) and amplitude (open symbols) $\Delta\theta_0/\theta_S$ of the laser-induced precession as a a function of φ_{H} measured for an external magnetic field of $H_{\text{ext}} = 0.26$ T. (c) z component of the torque $\mathbf{T}_0$ (4) calculated as a function of φ_{H} for the case when $\Delta K_i = 2\Delta K_{yz}$. Note that the abrupt change of the initial phase ξ_0 observed at $\varphi_{\text{H}} = 180°$ occurs because the effective anisotropy field H_a jumps to another equilibrium position when $\varphi_{\text{H}} > 180°$.

Nevertheless, the initial phase as well as the amplitude of the excited precession are essentially independent from the pump polarization azimuthal angle ϕ, which rules out the inverse Cotton-Mouton [56] as well as the photomagnetic effect [26].

Polarization-independent excitation of the magnetization precession is often driven by the laser-induced demagnetization which affects $\mathbf{H}_{\text{eff}}$ via modification of $\mathbf{H}_{\text{d}}$ (2). This mechanism can be safely ruled out in our experiment, since the laser-induced demagnetization in the studied film at the considered pump photon energies is the slow process with the characteristic time of ~500 ps (see Appendix B). On the other hand, the observed precession excitation could occur via fast laser-induced changes of the magnetic anisotropy parameters.

In order to test this hypothesis we have studied in more detail the laser-induced excitation of the precession in the magnetic field of $H_{\text{ext}} = 0.26$ T applied at different azimuthal angles in the range $10° < \varphi_{\text{H}} < 190°$ [Fig. 7(a)] [69]. A weak applied field of 0.26 T has been chosen in order to maximize the contribution to the precession excitation originating from the field-dependent mechanism. Figure 7(b) shows the amplitude and the initial phase ξ_0 of the precession as a function of the azimuthal angle φ_{H}. As one can see, ξ_0 is gradually changing by more than $\pi/2$ in the range $80° < \varphi_{\text{H}} < 170°$. This experiment clearly demonstrates that the initial phase of the precession is very sensitive to the orientation of the applied magnetic field and, thus, to the equilibrium orientation of the magnetization with respect to the sample axes.

We note that the change of the anisotropy parameters can be considered as a displacive mechanism of the precession excitation when the spin system reacts to the changes of $\mathbf{H}_{\text{eff}}$ direction under the effect of the laser pulse [56]. In this case, the phase $\xi_0 = 0$ of the oscillations of the z component of the magnetization (cosinelike temporal dependence) indicates that the corresponding initial torque vector $\mathbf{T}_0$ is directed in the xy plane, i.e., the z component of $\mathbf{H}_{\text{eff}}$ has been altered. The phase $\xi_0 = \pi/2$ corresponds to the situation, when the excitation leads to the change of the component of the effective field in the xy plane. Consequently, the laser-induced torque $\mathbf{T}_0$ acting on the magnetization is directed along the z axis. Thus, it can be seen from Figs. 7(a) and 7(b) that the torque $\mathbf{T}_0$ changes its direction and strength.

In Table I we present the components of the torque $\mathbf{T}_0$ (4) as a function of the polar ψ_{M} and azimuthal φ_{M} angles of the magnetization. These expressions allow us to eliminate the change of the K_u parameter as a major driving mechanism for the precession excitation. Indeed, for any orientation of the magnetization ΔK_u does not affect the z component of the torque $\mathbf{T}_0$. In this case the initial phase ξ_0 of the M_z oscillations is expected to be 0 with no pronounced dependence on φ_{H}. This strongly contradicts the experimental data in Fig. 7(b), where the initial phase ξ_0 spans over a range exceeding $\pi/2$, thus indicating that at least for some directions of the applied magnetic field the T_z component is nonzero.

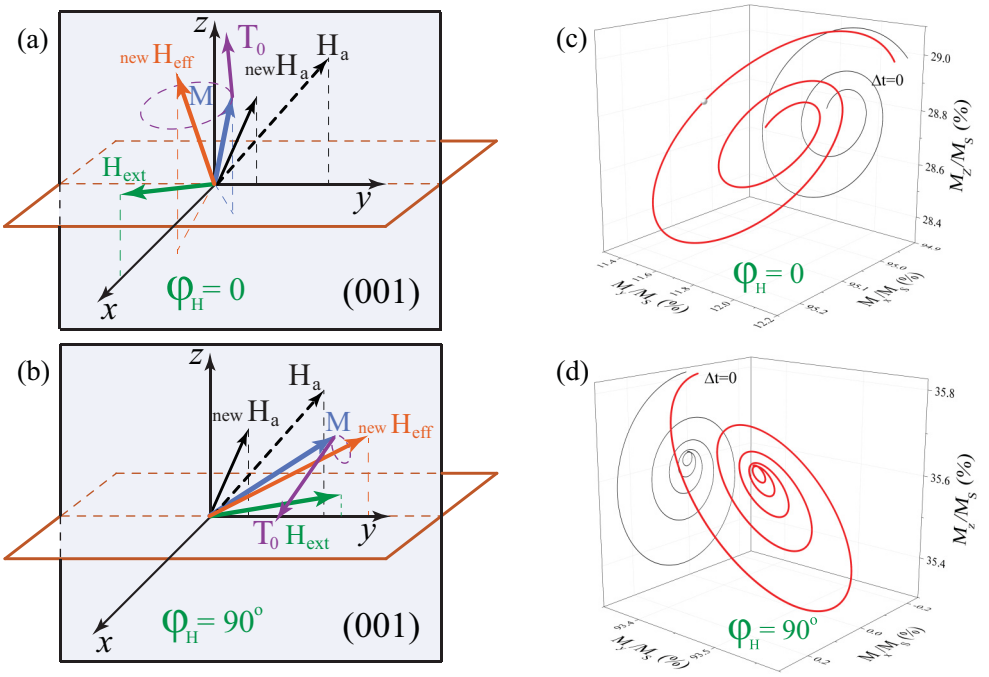

FIG. 8. Graphical illustration of the process of pulse-induced magnetic anisotropy change with the following precessional dynamics for (a), (c) $\varphi_H = 0$ and (b), (d) $\varphi_H = 90°$. Cases (c) and (d) depict magnetization trajectory after the excitation calculated using parameters as in Fig. 4. Note that in the case (b), (d), the effective anisotropy field and the applied field both lie in the yz plane. As a result, induced change of the anisotropy parameters does not deflect the net effective field away from this plane. This prevents the appearance of the z component of the induced torque $\mathbf{T}_0$. By contrast, when the applied field is perpendicular to the yz plane, the same change of the anisotropy modifies both deflection of $\mathbf{H}_{\text{eff}}$ from the yz plane and its orientation in the plane. As a result, all three components of the induced torque $\mathbf{T_0}$ should be finite.

Another important conclusion which can be drawn from the results shown in Fig. 7(b) is that the initial phase ξ_0 is close to zero when the azimuthal angle is $\varphi_H = 90°$. Note, that in this case both the effective anisotropy field $\mathbf{H}_a$ and the applied magnetic field lie in the yz easy plane [see Fig. 1(a)]. In this geometry, the net effective field $\mathbf{H}_{\text{eff}}$ should remain in the yz plane even if the laser-induced changes of any of the anisotropy parameters ΔK occur. This, in turn, corresponds to the initial phase $\xi_0 = 0$ of the laser-induced precession, in agreement with the experiment. Panels (a) and (b) of Fig. 8 show schematically the moment of precession launching in the cases $\varphi_H = 0$ and $\varphi_H = 90°$, and demonstrate the change of the initial phase of the magnetization precession as the azimuthal angle φ_H varies.

As one can see from the data presented in Figs. 7(a) and 7(b), there is a clear decrease of the amplitude of the excited precession as the φ_H is changed from 10° to 170°. It can be easily understood, taking into account that the azimuthal angle of magnetization varies from a value $10° < \varphi_M < 90°$ to $90° < \varphi_M < 170°$. The polar angle of magnetization varies as well, remaining in the range of $0° < \psi < 90°$. Then, from the expressions listed in Table I one can see that such a change of the magnetization directional angles results in the sign change of some, but not all components of the torque $\mathbf{T}_0$, exerted due to laser-induced anisotropy modification. This leads to the change of the magnitude of the laser-induced torque $\mathbf{T}_0$ and, thus, of the precession amplitude.

In order to further substantiate the suggested mechanism of the precession excitation, we have modeled the changes of the different components of the torque $\mathbf{T}_0$ (4) as functions of ΔK_u, ΔK_i, or ΔK_{yz} induced by the pump pulse. The calculations were performed taking anisotropy parameters obtained for this film. The equilibrium orientation of the magnetization (ψ_M, φ_M) has been calculated using these parameters for each direction of $\mathbf{H}_{\text{ext}}$ in the range of $10° < \varphi_H < 190°$. Then the laser-induced torque $\mathbf{T}_0$ (4) has been calculated assuming changes of K_i or K_{yz} anisotropy parameters. For the sake of clarity the torque occurring due to the ultrafast inverse Faraday effect was neglected. Figure 7(c) shows the z component of the torque $\mathbf{T}_0$ (4) as a function of φ_H for the case when the laser-induced decrease of the orthorhombic anisotropy parameter ΔK_{yz} is twice as large as the change of the in-plane uniaxial parameter ΔK_i. As one can see, the outcome of this model agrees with the experimental results. In fact, the variations of the calculated z component of the torque $\mathbf{T}_0$ [Fig. 7(c)] correlate with the changes of the initial phase of the precession ξ_0 [Fig. 7(b)]. In Figs. 8(c) and 8(d) we show in detail the calculated [Eq. (3)] time-dependent trajectory of the magnetization upon a sudden change of anisotropy parameters in two distinct situations, $\varphi_H = 0$ and $\varphi_H = 90°$. Obtained trajectories agree with the experimental results and reproduce the cosinelike variations of M_z when $\varphi_H = 90°$. We note that although the z component of the torque $\mathbf{T}_0$ vanishes for certain angles φ_H the total torque remains always

nonzero. This is supported by the experimental observations that for any azimuthal angle in the range $10^\circ < \varphi_H < 190^\circ$ the magnetization precession is always excited. In Figs. 4(c) and 4(d) we show the change of M_z as a function of the time delay, calculated using the LLG equation and taking into account both the ultrafast IFE and the change of anisotropy parameters. As can be seen, we successfully reproduce the field and polarization dependencies of the excited precession [Figs. 4(a) and 4(b)].

The above-described analysis allows us to conclude that the field-dependent excitation of the magnetization precession occurs via the ultrafast change of the growth-induced anisotropy parameters. Since this change is independent from the laser pulse linear polarization [Fig. 6(c)], we argue that the heating can be a plausible mechanism underlying the process. Indeed, various parameters of the growth-induced anisotropy are known to be temperature dependent [70,71]. Thus, the increase of the lattice temperature in magnetic dielectrics on a picosecond time scale following the absorption of the fraction of the femtosecond laser pulse energy, should affect the magnetic anisotropy on the same time scale. The growth-induced anisotropy parameters exhibit distinct temperature dependencies, and, as a result, they change differently in response to the heating. The subsequent cooling of the lattice relies on the much slower heat dissipation. Consequently, the relaxation of the effective anisotropy field to its equilibrium value is expected to be the slow process, in agreement with the displacive character of the change of the anisotropy parameters.

For the pump fluence of 10 $\mathrm{mJ/cm^{-2}}$ we estimated the lattice temperature increase to be of $\Delta T \sim 1$ K, taking the heat capacity of a Bi-substituted iron garnet of $3.85\,\mathrm{J\,cm^{-3}\,K^{-1}}$ [72]. To verify whether such a small temperature increase ΔT could lead to the anisotropy change, we used the phenomenological relation between the temperature-dependent magnetization and the uniaxial magnetic anisotropy [70]:

$$1 + \frac{\Delta K_u(\Delta T)}{K_u} = \left(1 + \frac{\Delta M_S(\Delta T)}{M_S}\right)^3, \tag{9}$$

In our sample, demagnetization amounts to $\Delta M_S/M_S \approx -0.2\%$ (see Appendix B) and can be used as a measure of total ΔT occurred due to laser pulse excitation. Then Eq. (9) yields that the anisotropy change for the same increase of the temperature is of $\Delta K_u/K_u \approx -0.6\%$. This is of the same order of magnitude that we used in our modeling [Figs. 4(c) and 4(d) and 8(c) and 8(d)].

In order to confirm the conclusion about the thermal origin of the laser-induced anisotropy change, we made a series of experiments with different pump photon energy. This allowed us to study the precession excitation when the absorption coefficient for the pump pulses varies [see inset in Fig. 6(b)]. The latter leads to different levels of ultrafast lattice heating achieved at the same excitation energy. Hence we expect the increase of the precession amplitude as the pump photon energy rises. Figure 6(a) shows pump-induced normalized probe polarization rotation as a function of time delay Δt at $H_{ext} = 0.26$ T for different pump photon energy E_p. Precession amplitudes presented in Fig. 6(b) are extracted from the fit of the experimental data to the function (7). The precession amplitude rises with absorption, as expected, with one exception at the highest absorption at $E_p = 2$ eV. In our opinion this deviation from a monotonous increase may originate from nonuniform excitation due to the high absorption. Similar deviation from the monotonously increasing trend of the precession amplitude dependence on the pump pulse absorbtion was also observed in Ref. [65], and was ascribed to generation of magnetostatic spin waves. Note, in our experiments optical transmission change also gradually increases with an increase of absorption, except in the case of the highest absorption coefficient, indicating that some optical nonlinear effects may start to play a role at this absorption level.

We note that the polarization-independent excitation of the magnetization precession in garnet films has been also reported in Refs. [40,62]. Both studies were carried out on the films grown on high-symmetry (001)-type GGG substrates and possessing easy-plane-type anisotropy, with no pronounced in-plane anisotropy. In Ref. [62] it has been shown that the polarization-independent contribution to the precession excitation occurs with magnetic field being deflected from the sample plane. The authors have interpreted the mechanism of the precession excitation as the nonthermal photoinduced anisotropy. Nevertheless, we suggest that the thermal change of the anisotropy could also contribute to the excitation process. However, distinguishing this mechanism from the others would be challenging, since the (001)-type films do not allow for experimental studies, where the torque occurring due to the laser-induced thermal changes of magnetic anisotropy possesses strong dependence on the applied field orientation (Figs. 7 and 8).

The demagnetization induced in dielectric garnet films by a pump pulse, due to heating, is mediated by the relatively slow phonon-magnon interaction. As we show [see Appendix B and Fig. 10(b) therein], the demagnetization in the garnet films upon optical excitation in a range of moderate absorption occurs on the time scale of ~500 ps. Therefore, the demagnetization itself cannot contribute to the excitation of the precession; however, it does contribute to the observed probe polarization dynamics. In our experimental geometry the static M_z component is finite in the whole range of the applied fields [see Fig. 2(a)]. Therefore, the demagnetization in the sample under consideration, analogous to that observed in the film with much stronger anisotropy, should manifest itself as a slow change in the rotation of the probe polarization. As one can see from Fig. 4(b), there is a slow change of the induced probe polarization with a characteristic time of ~500 ps. This slow process depends on the sign of the applied field, does not depend on the pump polarization, and is stronger in the range of low magnetic fields. This contribution to the signal is the manifestation of the laser-induced demagnetization. The character of the time delay dependence of the z component of the magnetization is somewhat more intricate than the exponential decay, found in the film with strong anisotropy [Fig. 10(b)]. Possibly, the change of the magnetization value, which follows the function (B1), is accompanied by the change of the effective anisotropy field (2). As a result, the change of M_z can deviate from the exponential behavior (B1).

VI. CONCLUSIONS

In conclusion, we investigated the interaction between femtosecond laser pulses and thin ferrimagnetic substituted iron garnet film grown on a low-symmetry (210)-type GGG substrate. We show experimentally that the effect of a laser pulse results in magnetization precession. Using pump pulses with various polarizations we demonstrated that the precession is in fact excited via two distinct mechanisms. The first one is the ultrafast inverse Faraday effect, which is found by now in a large number of magnetic dielectrics. Competing with this mechanism, is the change of the growth-induced anisotropy. Lack of the pump polarization dependence, as well as slow relaxation time of this mechanism indicate that there is a thermal change of the magnetic anisotropy, triggered by a rapid increase of the lattice temperature. We note that, in contrast to laser-induced dynamics in magnetic metals, this excitation does not rely on the much slower demagnetization.

The excitation of the magnetization precession in magnetic dielectrics via thermal change of the anisotropy has been previously explored only in the vicinity of the orientation phase transitions, where the anisotropy is strongly temperature dependent. Here we show that even far from the phase transition region the ultrafast heating of the lattice, resulting in the anisotropy change, can effectively excite the magnetization precession. Interestingly, the amplitude of the precession, excited via this mechanism is comparable to that occurring due to the IFE, which is expected to be pronounced in the studied garnet films. Furthermore, the relative contributions from these mechanisms can be changed by varying the applied magnetic field. As a result, one can gradually control the initial phase of the precession and its sensitivity to the polarization of the exciting laser pulse.

As we demonstrated experimentally and phenomenologically, the parameters of the magnetization precession excited via ultrafast change of the anisotropy are sensitive to the orientation of the applied magnetic field. Most importantly, the initial phase of the precession changes drastically, depending on the angle of the field with the easy plane of the magnetization. This suggests that the ultrafast change of the magnetic anisotropy should always be considered when one deals with the precession excited by femtosecond laser pulses in a dielectric placed in an external magnetic field not collinear with the easy magnetization direction.

ACKNOWLEDGMENTS

This work was performed at Ferroics Physics Laboratory of the Ioffe Institute (Russian Government Programm P220, Grant No. 14.B25.31.0025). Experiments were performed under the support of Russian Foundation for Basic Research (Grants No. 15-02-09052-a and No. 16-02-00377-a). Analytical work and spectral studies were performed by L.A.S., P.Y.S., and A. M. K. under the support of the Russian Science Foundation (Grant No. 16-12-10485). We thank M. P. Scheglov for the x-ray diffraction characterization of the samples, M. V. Zamoryanskaya for the XRF characterization, M. P. Volkov for the magnetic characterization using the physical property measurement system, and L. V. Lutsev for performing the FMR measurements.

TABLE II. Total, growth-, and stress-induced anisotropy parameters of the studied film, as extracted from the experimental data and calculations.

	Total (K)	Growth (K^g)	Stress (K^s)
K_u (J/m^3)	-5×10^3	-7×10^3	2×10^3
K_i (J/m^3)	-3×10^3	-3.5×10^3	5×10^2
K_{yz} (J/m^3)	-8.7×10^3	-7.7×10^3	-1×10^3

APPENDIX A: EQUILIBRIUM GROWTH- AND STRESS-INDUCED ANISOTROPY OF THE (210)-FILM

Magnetic anisotropy of the garnet film grown on a substrate of arbitrary orientation and characterized by a pronounced growth- and/or stress-induced anisotropy can be found from the two-parameter model [15,73]:

$$w_a = A\left(\alpha_{x'}^2\beta_{x'}^2 + \alpha_{y'}^2\beta_{y'}^2 + \alpha_{z'}^2\beta_{z'}^2\right) + B(\alpha_{x'}\alpha_{y'}\beta_{x'}\beta_{y'} + \alpha_{y'}\alpha_{z'}\beta_{y'}\beta_{z'} + \alpha_{z'}\alpha_{x'}\beta_{z'}\beta_{x'}), \tag{A1}$$

where α_i and β_i are directional cosines of magnetization $\mathbf{M}$ and the sample normal with respect to the crystallographic axes x', y', z'. By taking into account the growth direction [210] and making the transformation from the crystallographic axes to the coordinate frame xyz shown in Fig. 1, one finds the expression for the anisotropy parameters K entering Eq. (1):

$$\begin{aligned} K_u &\approx 0.67A + 0.16B; \\ K_i &\approx 0.67A - 0.16B; \\ K_{yz} &\approx 2.13K_u - 0.63K_i. \end{aligned} \tag{A2}$$

In order to estimate the values of the anisotropy parameters we have approximated the experimental field and azimuthal dependencies of the precessional frequency [Figs. 3(b) and 3(c)], and the field dependence of the Faraday rotation $\theta \sim M_z$ [Fig. 2(a)] using the analytical expression for magnetic energy [74,75]. The resulting curves are shown in the corresponding plots. The values of the anisotropy parameters providing good agreement between calculations and experimental data are given in Table II.

The magnetic anisotropy described by the parameters K has two contributions: the growth- (K^g) and the stress-induced (K^s) ones. Straightforward calculation of the growth-induced contribution to the magnetic anisotropy requires knowledge of a number of microscopical parameters, while the stress-induced one can be estimated from the phenomenological model. Magnetoelastic contributions to the magnetic anisotropy energy of the (210) iron garnet film can be expressed as [15]

$$\begin{aligned} K_u^s &= \tfrac{3}{2}\lambda_{100}\sigma_0\beta_1^2 + 3\lambda_{111}\sigma_0\beta_1^3\beta_2; \\ K_i^s &= \tfrac{3}{2}\lambda_{100}\sigma_0\beta_2^2 + 3\lambda_{111}\sigma_0\beta_1\beta_2^3; \\ K_{yz}^s &= -3\lambda_{100}\sigma_0\beta_1\beta_2, \end{aligned} \tag{A3}$$

where λ_{100} and λ_{111} are magnetostriction coefficients for the iron garnet film, and σ_0 is the biaxial stress arising due to the film/substrate lattice mismatch $\Delta a_0/a_0$. For garnets, characterized by the Young's modulus of $\sim 2\times10^{11}$ N/m^2 the

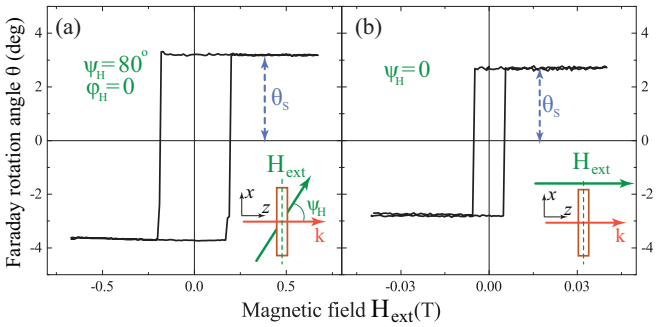

FIG. 9. Static Faraday rotation as a function of the external magnetic field in the film with strong anisotropy with external field applied at (a) $\psi_H = 80^\circ$ and (b) $\psi_H = 0$. θ_s denotes the Faraday rotation at remanence, which is proportional to the samples magnetization M_S. Insets show the experimental geometries used for measuring the static Faraday rotation in the samples.

relation between the stress and the substrate/lattice mismatch $\Delta a_0/a_0$ is $\sigma_0 = 2.8 \times 10^{11} \Delta a_0/a_0$ Pa [76]. We estimated the stress-induced contribution to the magnetic anisotropy, taking the lattice mismatch in the studied film $\Delta a_0/a_0 = -0.38\%$ and the typical magnetostriction coefficients for the garnets $\sim -10^{-6}$. Resulting stress-induced anisotropy parameters are given in Table II.

The values of the growth-induced anisotropy parameters calculated as $K^g = K - K^s$ are listed in Table II. From comparison of the growth- and stress-induced parameters we can conclude that the growth-induced anisotropy dominates over the stress-induced one. This is in agreement with the literature data on substituted garnets with high (>1) Bi^{3+} content, in which growth-induced anisotropy energy can exceed 10^4 J/m^3 [15,51].

APPENDIX B: LASER-INDUCED DEMAGNETIZATION OF THE SUBSTITUTED IRON GARNET FILM

Laser-induced demagnetization, if it occurs on a relatively short time scale, can be a driving mechanism of the excitation of the magnetization precession. Therefore, we investigated the demagnetization triggered by the femtosecond laser pulses in order to evaluate the strength and the time scale of this process in the garnet film under study. For this we selected the film of composition $(Y_{1.17}Bi_{1.44}Pr_{0.26}Lu_{0.24})(Fe_{3.66}Ga_{1.23})O_{12}$, which is characterized by the strong out-of-plane anisotropy. Figure 9 shows the field dependences of the Faraday rotation measured in the same geometries as in Fig. 2. As one can see, available external field applied at the $\psi_H = 80^\circ$ with respect to the sample normal is not sufficient to deflect the magnetization from the easy axis [Fig. 9(a)]. In such film in the experimental geometry, used for the pump-probe studies [Fig. 1(b)] with the field applied at $\psi_H = 80^\circ$, we probe solely the change of the magnetization magnitude while other processes such as magnetization precession are not detected even if excited. Therefore, such experiment is the most suitable for detecting laser-induced demagnetization via the Faraday rotation.

Dependencies of the polarization rotation of the probe pulse as a function of the pump-probe time delay Δt are shown in Fig. 10(a) for the two opposite applied magnetic fields

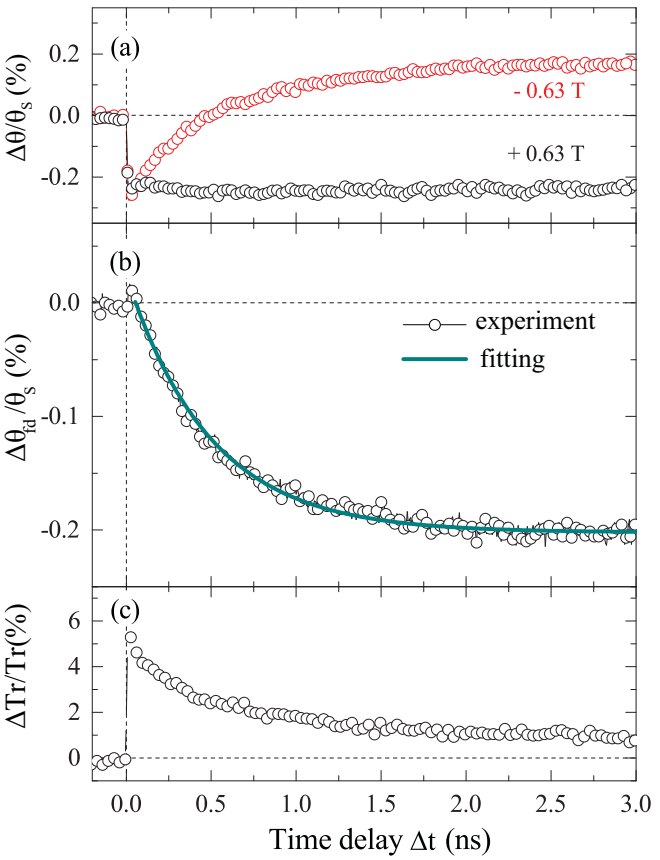

FIG. 10. (a) Normalized rotation of the probe polarization induced by the linearly polarized laser pulse as a function of the pump-probe time delay Δt measured for positive and negative magnetic field of ± 0.63 T in the film with strong anisotropy. (b) Field-dependent contribution to the laser-induced dynamics, extracted using Eq. (6) from the data shown in the panel (a) (symbols). Solid line is a fit using Eq. (B1). (c) Normalized change of the sample transmission as a function of pump-probe time delay Δt.

exceeding the saturation field. Figure 10(a) shows that the dynamics notably changes as the $\mathbf{H}_{ext}$ is reversed. In order to analyze this behavior we extracted the sign-dependent contribution (6) from the measured signals, which can be reliably considered as a measure of the pump-induced change of M_z. We note that such approach excludes the sign-independent contribution. Time evolution of the latter (not shown) closely resembles the temporal transmission changes ΔTr/Tr caused by pump shown in Fig. 10(c). Therefore, we attribute this contribution to the changes of optical or magneto-optical sample properties but not to the alteration of the magnetization magnitude or its orientation.

The time-delay dependence of the signal $\Delta\theta_{fd}(t)/\theta_s \sim \Delta M_z(t)/M_s$ has been fitted by a function

$$\frac{\Delta\theta_{fd}(t)}{\theta_s} = \frac{\Delta\theta^0_{fd}}{\theta_s}(e^{-t/\tau_{dm}} - 1), \tag{B1}$$

yielding the characteristic time $\tau_{dm} = 500 \pm 5$ ps. The value $\Delta\theta^0_{fd}/\theta_s$ characterizes the magnitude of this process and amounts to 0.2%. Noting that the magnetization is directed along the sample normal, we conclude from the experimental

data that the action of the pump pulses induces slow exponential change of the magnetization magnitude.

The long time scale of 500 ps and small magnitude of 0.2% of the observed change of the magnetization suggest that pump pulses trigger the demagnetization in the sample. Such a process in magnetically ordered dielectrics was reported in Ref. [58] and studied for the case of ferro- and ferrimagnetic [59,62], weak ferromagnetic [58], and antiferromagnetic [77] materials. This process can be understood as follows. Optical absorption of a laser pulse leads to excitation of electrons to the excited states $3d$ of the Fe^{3+} ions which decays at the femtosecond time scale leading to nonequilibrium phonon excitation and subsequent increase of the lattice temperature [78]. Relatively weak phonon-magnon interaction mediates energy transfer from lattice to incoherent magnons thus increasing the effective spin temperature. This appears as a decrease of magnetization magnitude.

We would like to note that the slow change of the magnetization value can, in general, lead to the deviation of the magnetization from its equilibrium orientation resulting in a change of M_z. Indeed, the orientation of the magnetization is defined by the balance between the magnetic anisotropy energy w_a, the shape anisotropy energy $-4\pi M_z^2$, and the Zeeman energy $-\mathbf{M}\cdot\mathbf{H}_\mathrm{ext}$. While the anisotropy energy depends on the normalized components m_k of the magnetization but not on their absolute values [see Eq. (1)], the two other energies would decrease as the absolute magnitude of the magnetization decreases. As a result, the relative contribution of the magnetic anisotropy w_a grows. If the easy-axis anisotropy energy is comparable to the Zeeman energy the demagnetization would lead to the increase of M_z competing with a decrease of M_S. The described process is not expected to give any noticeable contribution in the film under consideration due to the dominance of the easy-axis anisotropy.

[1] G. Winkler, *Magnetic Garnets* (Fried. Vieweg & Sohn, Braunschweig, 1981).

[2] *Physics of Magnetic Garnets*, edited by A. Paoletti, Enrico Fermi International School of Physics (North-Holland, Amsterdam, 1978).

[3] A. G. Gurevich and G. A. Melkov, *Magnetization Oscillations and Waves* (CRC Press, Boca Raton, FL, 1996).

[4] E. G. Spencer and R. C. LeCraw, Phys. Rev. Lett. **1**, 241 (1958).

[5] V. V. Pavlov, R. V. Pisarev, A. Kirilyuk, and T. Rasing, Phys. Rev. Lett. **78**, 2004 (1997).

[6] V. N. Gridnev, V. V. Pavlov, R. V. Pisarev, A. Kirilyuk, and T. Rasing, Phys. Rev. B **63**, 184407 (2001).

[7] B. B. Krichevtsov, V. V. Pavlov, and R. V. Pisarev, Pis'ma Zh. Eksp. Teor. Fiz. **49**, 466 (1989) [Sov. Phys. JETP Lett. **49**, 535 (1989)].

[8] A. S. Logginov, G. A. Meshkov, A. V. Nikolaev, and A. P. Pyatakov, Pis'ma Zh. Eksp. Teor. Fiz. **86**, 124 (2007) [JETP Lett. **86**, 115 (2007)].

[9] A. I. Popov, D. I. Plokhov, and A. K. Zvezdin, Phys. Rev. B **90**, 214427 (2014).

[10] Y. K. Fetisov and G. Srinivasan, Appl. Phys. Lett. **88**, 143503 (2006).

[11] P. K. Tien, R. J. Martin, R. Wolfe, R. C. Le Craw, and S. L. Blank, Appl. Phys. Lett. **21**, 394 (1972).

[12] M. Inoue, R. Fujikawa, A. Baryshev, A. B. Khanikaev, P. B. Lim, H. Uchida, O. A. Aktsipetrov, A. A. Fedyanin, T. V. Murzina, and A. B. Granovsky, J. Phys. D: Appl. Phys. **39**, R151 (2006).

[13] G. Armelles, A. Cebollada, A. García-Martín, and M. U. González, Adv. Opt. Mater. **1**, 10 (2013).

[14] A. L. Chekhov, A. I. Stognij, T. Satoh, T. V. Murzina, I. Razdolski, and A. Stupakiewicz, arXiv:1712.01617.

[15] A. H. Eschenfelder, *Magnetic Bubble Technology* (Springer-Verlag, Berlin, 1981).

[16] A. P. Malozemoff and J. C. Slonczewski, *Magnetic Domain Walls in Bubble Materials* (Academic, New York, 1979).

[17] N. Ogawa, W. Koshibae, A. J. Beekman, N. Nagaosa, M. Kubota, M. Kawasaki, and Y. Tokura, Proc. Natl. Acad. Sci. USA **112**, 8977 (2015).

[18] A. P. Pyatakov, A. S. Sergeev, E. P. Nikolaeva, T. B. Kosykh, A. V. Nikolaev, K. A. Zvezdin, and A. K. Zvezdin, Usp. Fiz. Nauk **185**, 1077 (2015) [Phys. Usp. **58**, 981 (2015)].

[19] N. E. Khokhlov, A. E. Khramova, E. P. Nikolaeva, T. B. Kosykh, A. V. Nikolaev, A. K. Zvezdin, A. P. Pyatakov, and V. I. Belotelov, Sci. Rep. **7**, 264 (2017).

[20] V. V. Kruglyak, S. O. Demokritov, and D. Grundler, J. Phys. D: Appl. Phys. **43**, 264001 (2010).

[21] A. A. Serga, A. V. Chumak, and B. Hillebrands, J. Phys. D: Appl. Phys. **43**, 264002 (2010).

[22] H. Nakayama, M. Althammer, Y.-T. Chen, K. Uchida, Y. Kajiwara, D. Kikuchi, T. Ohtani, S. Geprägs, M. Opel, S. Takahashi, R. Gross, G. E. W. Bauer, S. T. B. Goennenwein, and E. Saitoh, Phys. Rev. Lett. **110**, 206601 (2013).

[23] M. Tekielak, W. Andra, A. Maziewski, and J. Taubert, J. Phys. IV **7**, C1-461 (1997).

[24] M. Borovets, A. A. Garmonov, S. G. Rudov, and Y. M. Fedorov, Pis'ma Zh. Eksp. Teor. Fiz. **50**, 431 (1989) [Sov. Phys. JETP Lett. **50**, 466 (1989)].

[25] A. B. Chizhik, I. I. Davidenko, A. Maziewski, and A. Stupakiewicz, Phys. Rev. B **57**, 14366 (1998).

[26] F. Hansteen, A. V. Kimel, A. Kirilyuk, and T. Rasing, Phys. Rev. Lett. **95**, 047402 (2005).

[27] A. V. Kimel, A. Kirilyuk, A. Tsvetkov, R. V. Pisarev, and T. Rasing, Nature (London) **429**, 850 (2004).

[28] A. Caretta, M. C. Donker, A. O. Polyakov, T. T. M. Palstra, and P. H. M. van Loosdrecht, Phys. Rev. B **91**, 020405(R) (2015).

[29] A. Stupakiewicz, K. Szerenos, D. Afanasiev, A. Kirilyuk, and A. V. Kimel, Nature (London) **542**, 71 (2017).

[30] Y. Hashimoto, S. Kobayashi, and H. Munekata, Phys. Rev. Lett. **100**, 067202 (2008).

[31] A. V. Scherbakov, A. S. Salasyuk, A. V. Akimov, X. Liu, M. Bombeck, C. Brüggemann, D. R. Yakovlev, V. F. Sapega, J. K. Furdyna, and M. Bayer, Phys. Rev. Lett. **105**, 117204 (2010).

[32] M. van Kampen, C. Jozsa, J. T. Kohlhepp, P. LeClair, L. Lagae, W. J. M. de Jonge, and B. Koopmans, Phys. Rev. Lett. **88**, 227201 (2002).

[33] E. Carpene, E. Mancini, D. Dazzi, C. Dallera, E. Puppin, and S. de Silvestri, Phys. Rev. B **81**, 060415(R) (2010).

[34] V. N. Kats, T. L. Linnik, A. S. Salasyuk, A. W. Rushforth, M. Wang, P. Wadley, A. V. Akimov, S. A. Cavill, V. Holy, A. M. Kalashnikova, and A. V. Scherbakov, Phys. Rev. B **93**, 214422 (2016).

[35] R. Wilks, R. J. Hicken, M. Ali, and B. J. Hickey, J. Appl. Phys. **97**, 10A705 (2005).

[36] J. Hohlfeld, E. Matthias, R. Knorren, and K. H. Bennemann, Phys. Rev. Lett. **78**, 4861 (1997).

[37] C. Stamm, T. Kachel, N. Pontius, R. Mitzner, T. Quast, K. Holldack, S. Khan, C. Lupulescu, E. F. Aziz, M. Wietstruk, H. A. Dürr, and W. Eberhardt, Nat. Mater. **6**, 740 (2007).

[38] F. Atoneche, A. M. Kalashnikova, A. V. Kimel, A. Stupakiewicz, A. Maziewski, A. Kirilyuk, and T. Rasing, Phys. Rev. B **81**, 214440 (2010).

[39] I. Yoshimine, T. Satoh, R. Iida, A. Stupakiewicz, A. Maziewski, and T. Shimura, J. Appl. Phys. **116**, 043907 (2014).

[40] B. Koene, M. Deb, E. Popova, N. Keller, T. Rasing, and A. Kirilyuk, Phys. Rev. B **91**, 184415 (2015).

[41] A. V. Kimel, B. A. Ivanov, R. V. Pisarev, P. A. Usachev, A. Kirilyuk, and T. Rasing, Nat. Phys. **5**, 727 (2009).

[42] J. A. de Jong, I. Razdolski, A. M. Kalashnikova, R. V. Pisarev, A. M. Balbashov, A. Kirilyuk, T. Rasing, and A. V. Kimel, Phys. Rev. Lett. **108**, 157601 (2012).

[43] D. Afanasiev, B. A. Ivanov, A. Kirilyuk, T. Rasing, R. V. Pisarev, and A. V. Kimel, Phys. Rev. Lett. **116**, 097401 (2016).

[44] T. Satoh, Y. Terui, R. Moriya, B. A. Ivanov, K. Ando, E. Saitoh, T. Shimura, and K. Kuroda, Nat. Photonics **6**, 662 (2012).

[45] V. I. Belotelov and A. K. Zvezdin, Phys. Rev. B **86**, 155133 (2012).

[46] D. Bossini, V. I. Belotelov, A. K. Zvezdin, A. N. Kalish, and A. V. Kimel, ACS Photonics **3**, 1385 (2016).

[47] J. A. de Jong, A. V. Kimel, R. V. Pisarev, A. Kirilyuk, and T. Rasing, Phys. Rev. B **84**, 104421 (2011).

[48] A. V. Kimel, C. D. Stanciu, P. A. Usachev, R. V. Pisarev, V. N. Gridnev, A. Kirilyuk, and T. Rasing, Phys. Rev. B **74**, 060403 (2006).

[49] G. V. Arzamastseva, A. M. Balbashov, F. V. Lisovskii, E. G. Mansvetova, A. G. Temiryazev, and M. P. Temiryazeva, Zh. Eksp. Teor. Fiz. **147**, 793 (2015) [J. Exp. Theor. Phys. **120**, 687 (2015)].

[50] I. Nistor, C. Holthaus, S. Tkachuk, I. D. Mayergoyz, and C. Krafft, J. Appl. Phys. **101**, 09C526 (2007).

[51] P. Hansen and K. Witter, J. Appl. Phys. **58**, 454 (1985).

[52] L. D. Landau and E. M. Lifshitz, Phys. Z. Sowjetunion **8**, 153 (1935).

[53] T. L. Gilbert, IEEE Trans. Magn. **40**, 3443 (2004).

[54] A. V. Kimel, A. Kirilyuk, P. A. Usachev, R. V. Pisarev, A. M. Balbashov, and T. Rasing, Nature (London) **435**, 655 (2005).

[55] A. M. Kalashnikova, A. V. Kimel, R. V. Pisarev, V. N. Gridnev, A. Kirilyuk, and T. Rasing, Phys. Rev. Lett. **99**, 167205 (2007).

[56] A. M. Kalashnikova, A. V. Kimel, R. V. Pisarev, V. N. Gridnev, P. A. Usachev, A. Kirilyuk, and T. Rasing, Phys. Rev. B **78**, 104301 (2008).

[57] V. N. Gridnev, Phys. Rev. B **77**, 094426 (2008).

[58] A. V. Kimel, R. V. Pisarev, J. Hohlfeld, and T. Rasing, Phys. Rev. Lett. **89**, 287401 (2002).

[59] T. Ogasawara, K. Ohgushi, Y. Tomioka, K. S. Takahashi, H. Okamoto, M. Kawasaki, and Y. Tokura, Phys. Rev. Lett. **94**, 087202 (2005).

[60] P. Hansen, K. Witter, and W. Tolksdorf, Phys. Rev. B **27**, 6608 (1983).

[61] A. Kirilyuk, A. V. Kimel, and T. Rasing, Rev. Mod. Phys. **82**, 2731 (2010).

[62] F. Hansteen, A. V. Kimel, A. Kirilyuk, and T. Rasing, Phys. Rev. B **73**, 014421 (2006).

[63] M. Jäckl, V. I. Belotelov, I. A. Akimov, I. V. Savochkin, D. R. Yakovlev, A. K. Zvezdin, and M. Bayer, Phys. Rev. X **7**, 021009 (2017).

[64] I. V. Savochkin, M. Jäckl, V. I. Belotelov, I. A. Akimov, M. A. Kozhaev, D. A. Sylgacheva, A. I. Chernov, A. N. Shaposhnikov, A. R. Prokopov, V. N. Berzhansky, D. R. Yakovlev, A. K. Zvezdin, and M. Bayer, Sci Rep. **7**, 5668 (2017).

[65] I. V. Savochkin, M. A. Kozhaev, A. I. Chernov, A. N. Kuzmichev, A. K. Zvezdin, and V. I. Belotelov, Fiz. Tv. Tela **59**, 883 (2017) [Phys. Solid State **59**, 904 (2017)].

[66] L. P. Pitaevskii, Zh. Eksp. Teor. Fiz. **39**, 1450 (1960) [Sov. Phys. JETP **12**, 1008 (1961)].

[67] P. S. Pershan, J. P. van der Ziel, and L. D. Malmstrom, Phys. Rev. **143**, 574 (1966).

[68] M. Pashkevich, A. Stupakiewicz, A. V. Kimel, A. Kirilyuk, A. Stognij, N. Novitskii, A. Maziewski, and T. Rasing, Europhys. Lett. **105**, 27006 (2014).

[69] T. P. Ma, S. F. Zhang, Y. Yang, Z. H. Chen, H. B. Zhao, and Y. Z. Wu, J. Appl. Phys. **117**, 013903 (2015).

[70] C. Zener, Phys. Rev. **96**, 1335 (1954).

[71] P. W. Shumate, Jr., D. H. Smith, and F. B. Hagedorn, J. Appl. Phys. **44**, 449 (1973).

[72] F. Inoue, A. Itoh, and K. Kawanishi, Jpn. J. Appl. Phys. **19**, 2105 (1980).

[73] E. M. Gyorgy, A. Rosencwaig, E. I. Blount, W. J. Tabor, and M. E. Lines, Appl. Phys. Lett. **18**, 479 (1971).

[74] H. Suhl, Phys. Rev. **97**, 555 (1955).

[75] J. O. Artman, Phys. Rev. **105**, 74 (1957).

[76] J. E. Davies and E. A. Giess, J. Mater. Sci. **10**, 2156 (1975).

[77] D. Bossini, A. M. Kalashnikova, R. V. Pisarev, T. Rasing, and A. V. Kimel, Phys. Rev. B **89**, 060405(R) (2014).

[78] G. B. Scott, D. E. Lacklison, and J. L. Page, Phys. Rev. B **10**, 971 (1974).